Theor Chem Account (2009) 122:87–100
DOI 10.1007/s00214-008-0487-7

REGULAR ARTICLE

Ab Initio rovibrational spectrum of the NaH_2^+ ion–quadrupole complex

Alister J. Page · Ellak I. von Nagy-Felsobuki

Received: 6 June 2008 / Accepted: 15 October 2008 / Published online: 12 November 2008

Abstract The electronic and rovibrational structure of ($^1A_1$) NaH_2^+ has been investigated using a relativistically-corrected, all-electron coupled-cluster with singles, doubles and perturbative triples (CCSD(T)) ansatz. For the electronic ground state this ansatz yielded equilibrium Na–H bond lengths (R_e) of 2.4208 Å and an equilibrium H–Na–H bond angle (θ_e) of 17.8°. An analytical potential energy surface (PES) was embedded in the rovibrational Hamiltonian. The PES was constructed using 118 CCSD(T) points and exhibited a residual error of 1.2 cm^{-1}. The rovibrational Hamiltonian was diagonalised using variational techniques. The vibrational and rovibrational eigenvectors were assigned using a configuration weight scheme in terms of normal modes and the Mulliken assignment scheme, respectively. For the ground vibrational state of ($^1A_1$) NaH_2^+, the vibration-averaged bond lengths $\langle R \rangle$ and angle $\langle \theta \rangle$ were 2.4995 Å and 17.1°, respectively. The ab initio ($^1A_1$) NaH_2^+ PES yielded a dissociation energy (D_0) value of 10.3 kJ mol^{-1}, which is in excellent agreement with the experimental value of 10.3 ± 0.8 kJ mol^{-1} (Bushnell et al. in J Phys Chem 98:2044, 1994). An analytical dipole moment surface was constructed using 90 CCSD(T) points. Rovibrational spectra of ($^1A_1$) NaH_2^+, ($^1A'$) $NaHD^+$ and ($^1A_1$) NaD_2^+ for $v \leq 10$, $J \leq 5$ were constructed using rovibrational transition moment matrix elements calculated in a novel manner that employs the analytical dipole moment surface (DMS). The rovibrational structure of the Na^+–H_2 $v_{HH} = 1 \leftarrow v_{HH} = 0$ band was calculated and compared to that of Li^+–H_2.

A. J. Page · E. I. von Nagy-Felsobuki (✉)
The Molecular Structure and Detection Group,
The University of Newcastle,
Callaghan, NSW 2308, Australia
e-mail: ellak@newcastle.edu.au

Keywords Potential energy surface · Dipole moment surface · Rovibrational spectrum · Molecular hydride cation

1 Introduction

Small molecular hydrides of the alkali metals have been assigned a central role in current models of primordial interstellar chemistries. In particular, the dihydrides of metals such as lithium, sodium and potassium have been the focus of several recent investigations. For example, it has been proposed that the chemical interaction between lithium and hydrogen was amongst the first to take place in the nascent universe ([1, 2] and references therein). Extensive efforts have therefore been made to characterise the nature of the lithium–hydrogen interaction [3]. The NaH_2 exciplex provides an archetypal example of an electronically non-adiabatic process. Such processes are of central importance to the study of photochemical reactions [3]. Hydrides of sodium and potassium also possess roles with respect to interstellar chemistry. For example, these metals have been identified in the spectra of dwarf stars and irradiated planets [4].

The structure and spectroscopy of small alkali metal-hydride cations is also of particular interest with respect to theory and experiment. There has been extensive investigation of the $^1A_1$ ground state of LiH_2^+ ([5, 6] and references therein), which exhibits a C_{2v} equilibrium structure and results from the interaction between the ion charge and the H_2 quadrupole moment. Despite this nature of the LiH_2^+ ground state interaction, this collision complex exhibits a rich spectroscopy. For example, Page and von Nagy-Felsobuki [5] and Kraemer and Špirko [6] recently reported the energies and radiative properties of bound and quasi-bound rovibrational states of ($^1A_1$) LiH_2^+

using ab initio methods. In addition, Bieske et al. [7, 8] recently unravelled the IR rovibrational spectra of LiH_2^+ and LiD_2^+ using mass-spectrometric techniques. Page and von Nagy-Felsobuki [5] reported ab initio rovibrational transition wavenumbers of LiD_2^+ in the D–D stretch band (at ca. 2,900 cm^{-1}) that were within ca. 5 cm^{-1} of the experimental values [8] for $K \leq 0$, 1, 2 and $J \leq 10$ (where K and J are the usual rotational quantum numbers [9]). These ab initio rovibrational transition wavenumbers were calculated using a full configuration interaction (FCI) ansatz in conjunction with triple-ζ basis sets.

The ground state of NaH_2^+ also results from an ion–quadrupole interaction, analagous to that of LiH_2^+. These species therefore exhibit similar structures and energetics. Nevertheless, there are fewer studies concerning the NaH_2^+ collision complex. For example, Switalski et al. [10] employed Hartree–Fock (HF) in conjunction with a model core potential to elucidate the equilibria of a number of two-electron valence systems including ($^1A_1$) NaH_2^+. In the only reported study concerning the ($^1A_1$) NaH_2^+ PES, Falcetta et al. [11] employed HF to construct a 291-point discrete PES grid which was represented analytically using a non-piecewise function. Curtiss and Pople [12] employed both HF and Møller-Plesset theory (MP4) in a theoretical investigation of the thermochemistry of the ground state of NaH_2^+. In the only experimental investigation of NaH_2^+, Bushnell et al. [13] reported $D_0(NaH_2^+)$ to be 10.3 ± 0.8 kJ mol^{-1}, 2.5 kJ mol^{-1} larger than the MP2/6-311G+(3*df*, 2*pd*) results (also reported by Bushnell et al.) More recently, Tamássy-Lentei and Szaniszló [14] employed a floating spherical Gaussian orbital ansatz to investigate the ground state structure and dissociation energetics of NaH_2^+. Barbatti et al. [15] employed MP2 and MP4 to characterise the ground state equilibria of $Na^+(H_2)_n$ (for $n \leq 7$) concluding that each species possessed thermodynamically stable structures. In 2005, Vitillo et al. [16] reported a detailed investigation of the ground state NaH_2^+ interaction, using both MP2/aug-cc-pVQZ and density functional theory. In general, calculations are in agreement with a minimum energy structure corresponding to a C_{2v} symmetry with bond lengths of ca. 2.5 Å and a bond angle of ca. 16°. A $^1\Sigma^+$ transition state has also been characterised in a number of theoretical studies [12, 16]. Analogous transition states have also been identified in MH_2^+ (M = Li, Na, K, Rb) [16] and MgH_2^{2+} [17]. Thus far in the literature, no PES or DMS have been constructed using a correlated ansatz for ($^1A_1$) NaH_2^+. Moreover, no experimental or theoretical investigation of the rovibrational spectroscopy of ($^1A_1$) NaH_2^+ has been reported to date.

We wish to report here ab initio rovibrational spectra of ($^1A_1$) NaH_2^+, ($^1A'$) $NaHD^+$ and ($^1A_1$) NaD_2^+, thus continuing our systematic study of the rovibrational spectra of metal dihydride cations [5, 17, 18]. A PES of ($^1A_1$) NaH_2^+ calculated using relativistically corrected coupled-cluster with singles, doubles and perturbative triples (CCSD(T)) has been developed and employed to calculate vibrational band origins and rovibrational transition wavenumbers. In a similar fashion, a CCSD(T) DMS has been constructed and embedded in the nuclear Hamiltonian. Vibrational and rovibrational radiative properties including radiative lifetimes, vibrational band strengths and rovibrational spectral intensities, have subsequently been calculated and moreover, are compared to rovibrational calculations of ($^1A_1$) LiH_2^+, the deuterated analog of which has been previously published [5]. All rovibrational properties of ($^1A_1$) LiH_2^+ and ($^1A_1$) NaH_2^+ have been calculated using fully variational algorithms. It is hoped that the data reported in this work will provide timely assistance for the spectroscopic identification and characterisation of ($^1A_1$) NaH_2^+, ($^1A'$)$NaHD^+$ and ($^1A_1$) NaH_2^+.

2 Computational details

The electronic ground state of NaH_2^+ has been investigated using all-electron relativistically-corrected CCSD(T). This ansatz has previously been described and validated with respect to the low-lying excited states of the neutral NaH_2 species [3]. The CCSD(T) wave function employed a HF determinant as a starting point. For Na and H, ANO-RCC [19] and aug-cc-pVQZ [20, 21] basis sets were employed, respectively. The former basis set is described explicitly as the [9*s*8*p*5*d*4*f*] contraction, and necessitates the inclusion of relativistic effects via the second order truncation of the Douglass–Kroll–Hess (DK2) [22, 23] one-electron Hamiltonian. Basis set superposition error (BSSE) was accounted for by the use of the site-site function counterpoise (SSFC) method of Wells and Wilson [24]. All reported dipole moments of ($^1A_1$) NaH_2^+ were calculated as the gradient of the electronic energy with respect to an applied external electric field. All electronic structure calculations presented in this work have been calculated using the Molpro program system [25], and were constructed in the C_s symmetry framework.

3 Rovibrational Hamiltonian

The C_{2v} rovibrational Hamiltonian employed in this work is the normal **t** coordinate operator of Carney et al. [26],

$$\hat{H}_{ab}^{\mathrm{RV}} = E_a\langle S\rangle_{ab} + \frac{1}{2}\langle A\rangle_{ab}\hat{\Pi}_x^2 + \frac{1}{2}\langle B\rangle_{ab}\hat{\Pi}_y^2 + \frac{1}{2}\langle C\rangle_{ab}\hat{\Pi}_z^2 + \frac{1}{2}\langle D\rangle_{ab}\left(\hat{\Pi}_x\hat{\Pi}_y + \hat{\Pi}_y\hat{\Pi}_x\right) + \frac{i}{\hbar}\langle F\rangle_{ab}\hat{\Pi}_z + \hat{V} \quad (1)$$

here, E_a is the energy of vibrational state $\langle a|$. The overlap integral between $\langle a|$ and $|b\rangle$ is given by the matrix

element $\langle S|_{ab}$. Similarly, for states $\langle a|$ and $|b\rangle$, $\langle A|_{ab}$, $\langle B|_{ab}$, $\langle C|_{ab}$ and $\langle D|_{ab}$ are the rotational constant matrices and $\langle F|_{ab}$ is the Coriolis coupling matrix. The angular momenta of the system (in the molecule-fixed frame of reference) in the x, y and z components are described by $\hat{\Pi}_x, \hat{\Pi}_y$ and $\hat{\Pi}_z$, respectively. The operator $\hat{V}$ is the embedded analytical potential energy function (*vide infra*), which is evaluated numerically using a quadrature scheme adapted from that of Harris, Engerholm and Gwinn (HEG) [27]. In all vibrational calculations the expansion of the Watson operator [28] was truncated at third order, whereas matrix elements of the kinetic energy, vibrational angular momenta and potential energy operators were calculated exactly. The validity of the truncation of the Watson operator has been previously established with respect to the vibrational states of H_3^+ [29]. For example, this truncation yields vibrational eigenvalues converged to within ca. 0.01 cm^{-1} for low-lying vibrational states of H_3^+.

The three dimensional (3D) vibrational eigenfunctions $|\Psi\rangle \equiv |ijk\rangle$ were constructed as a CI of three 1D basis functions ψ_i, ψ_j and ψ_k. Each of the latter are eigenfunctions of the 1D Schrödinger equation in the respective normal-coordinate, and were optimised using a numerical finite-element method (FEM) detailed elsewhere [30]. This FEM, based upon the Rayleigh–Ritz method [31], numerically solves each Schrödinger equation over a series of single discrete elements. The basis functions employed are the piecewise continuous Hermite cubic polynomials. These basis functions are identically zero outside of the element being considered. The nth 1D eigenvector is ultimately composed from the optimised basis functions over each finite-element. The corresponding eigenvalue obtained using this method is therefore correct to $O(h^6 n^8)$, where h is the finite-element length.

Each vibrational state $|ijk\rangle$ was constructed from a CI of $20 \times 20 \times 20$ 1D eigenfunctions. A list of 8,000 configurations therefore comprised each vibrational wave function. Each state was subsequently assigned using a 'configuration weight' assignment scheme, in which the relative contribution of each configuration is calculated via,

$$\text{weight}_{ij} = \frac{|C_{ij}|}{\left[\sum_{k=1}^{8,000} C_{ik}^2\right]^{1/2}} \tag{2}$$

where C_{ij} is the coefficient of the jth 1D basis function in the ith normalised 3D vibrational eigenfunction. Trial rovibrational eigenfunctions $|\Psi_{v,JKm}^{RV}\rangle$ were constructed as products between the optimised 3D vibrational eigenfunctions and $|R_{JKm}^{\pm}\rangle$ basis functions. The latter consists of plus-minus combinations of the symmetric-top eigenfunctions. This guarantees that all elements of the diagonalised rovibrational Hamiltonian remain real. Vibration-averaged

Table 1 Comparison of ($^1A_1$) NaH_2^+ equilibrium parameters

	R_e^a (Å)	$R_e(H_2)$ (°)	D_0 (kJ mol^{-1})	Harmonic wavenumbers (cm^{-1})		
				ω_1	ω_2	ω_3
SCF MO[b]	2.38	0.74				
HF[c]	2.541	0.732	10.3	260	4,577	439
HF[d]	2.458	0.739	7.2	306	4,518	558
HF[e]	2.475	0.740	8.0	286	4,522	502
MP2[f]	2.427	0.743	11.5			
MP2[g]	2.463	0.737	7.8	304	4,458	533
MP2[h]	2.45	0.7412	11.4			
CCSD(T)[i]	2.3918	0.7477	10.3	350	4,317	568
Experiment[g]			10.3 ± 0.8			

[a] Distance between Na^+ ion and H_2 bond midpoint

[b] In conjunction with a model core potential, see [10]

[c] In conjunction with 6-31G(*d*) basis sets, see [12]

[d] In conjunction with [3*s*, 2*p*] (H) and [6*s*, 5*p*, 1*d*] (Na) basis sets, see [35]

[e] In conjunction with [5*s*, 3*p*, 1*d*] (H) and 6-311G* (Na) basis sets, see [11]

[f] In conjunction with 6-311G(*d*, *p*) basis sets, see [15]. D_e value calculated using MP4 result

[g] In conjunction with 6-311G+(3*df*, 2*p*) basis sets, see [13]

[h] Includes BSSE correction, in conjunction with aug-cc-pVQZ basis sets. See [16]

[i] This work. D_0 value calculated using ZPE attained with the full vibrational wave function/PES. Harmonic wavenumbers calculated using numerical gradients with no BSSE correction, and are unscaled

structures of all vibrational states were calculated as the transformed expectation values of $\hat{H}_{ab}^{\mathrm{RV}}$ in the 1D eigenfunction basis. This procedure has been outlined previously [17, 32].

The 1D vibrational eigenfunctions of (^{1}A$_1$) NaH_2^+, (^{1}A′) $NaHD^+$ and (^{1}A$_1$) NaH_2^+ were calculated using a FEM grid consisting of 1,000 elements over the t_1 (a_1 breathe), t_2 (a_1 bend) and t_3 (b_2 asymmetric stretch) mode domains. These domains were [−3.0, 4.5 a.u.], [−0.75, 5.0 a.u.] and [−2.5, 2.5 a.u.], respectively. All 1D basis functions decayed appropriately in the classically forbidden regions of the PES. Moreover, it was ensured that all corresponding eigenvalues were converged to within the residual error of the PES.

4 Radiative properties

The vibrational transition moment integrals for states $|\Psi_a\rangle$ and $|\Psi_b\rangle$ were calculated using μ_x and μ_y component DMSs (*vide infra*), in conjunction with a novel adaptation of the HEG quadrature scheme [33]. In the 3D vibrational eigenfunction basis these integrals are of the form,

$$\mu_\alpha(a,b) = \langle ijk|\mu_\alpha(\rho_1,\rho_2,\rho_3)|lmn\rangle \tag{3}$$

where $\rho_1 = R^{\mathrm{e}} - R_1$, $\rho_2 = R^{\mathrm{e}} - R_2$, $\rho_3 = \theta^{\mathrm{e}} - \theta$ and $\alpha = x, y$. The variables R_1 and R_2 denote the instantaneous H_1–Na and Na–H_2 bond lengths, while θ denotes the instantaneous H_1–Na–H_2 bond angle. The Einstein coefficients of induced absorption (B_{ab}) and spontaneous emission (A_{ab}) were subsequently calculated,

$$B_{ab} = \frac{8\pi^3}{3h^2}\mu^2(a,b) \tag{4}$$

where B_{ab} and A_{ab} are such that,

$$N_a B_{ba}\rho_{\nu_{ab}} = N_b\left(A_{ab} + B_{ab}\rho_{\nu_{ab}}\right), \quad \frac{N_a}{N_b} = \frac{\left(A_{ba} + B_{ba}\rho_{\nu_{ab}}\right)}{B_{ab}\rho_{\nu_{ab}}} \tag{5}$$

at thermal equilibrium. Here, $\rho_{\nu_{ab}}$ is the spectral density of the external field at a given temperature T. The radiative lifetime of fluorescence and vibrational band intensity were calculated using,

$$\tau_b^f = \frac{1}{\sum_a A_{ba} + \sum_a B_{ba}\rho_{\nu_{ab}} + \sum_{b\prime} B_{bb\prime}\rho_{\nu_{ab}}} \tag{6}$$

and,

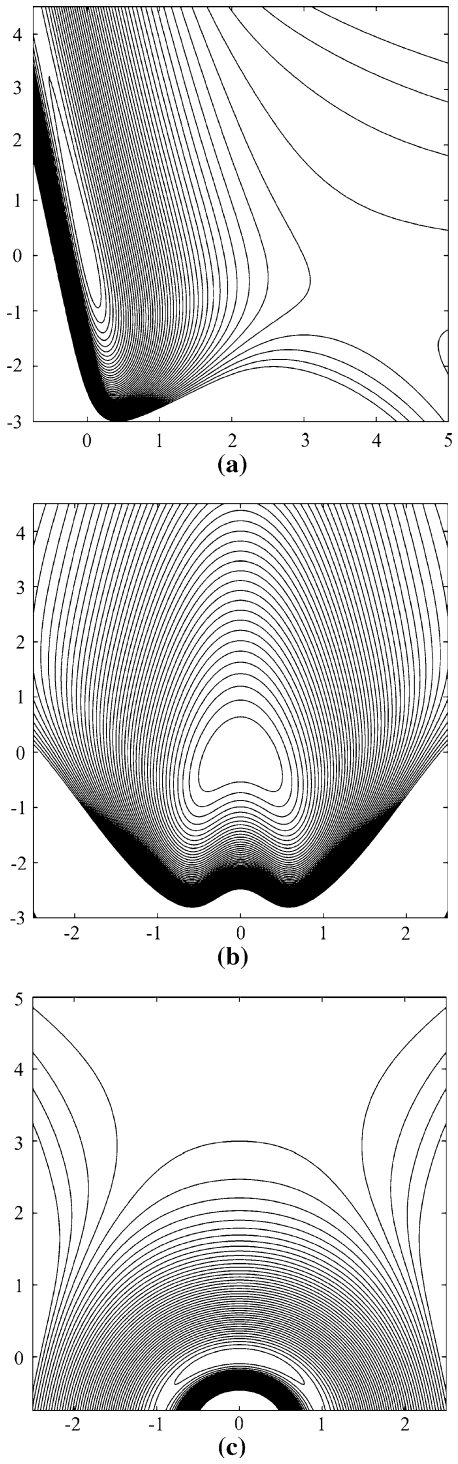

Fig. 1 Contour projections of the (^{1}A$_1$) NaH_2^+ CCSD(T) potential energy surface in terms of normal coordinates (a.u.): **a** t_2 (*horizontal axis*) vs. t_1 (*vertical axis*); **b** t_3 (*horizontal axis*) vs. t_1 (*vertical axis*); and **c** t_3 (*horizontal axis*) vs. t_2 (*vertical axis*). Contours spaced at 10 kJ mol^{-1}

Table 2 Padé expansion coefficients of the CCSD(T) potential energy surface

Expansion variable	Expansion coefficient[a]		Expansion variable	Expansion coefficient[a]	
	Numerator	Denominator		Numerator	Denominator
1	−163.3215260	−1.0	$\xi_1^4\xi_3 + \xi_2^4\xi_3$	1.5265894	0.0098367
$\xi_1 + \xi_2$	−21.5447690	−0.1319148	$\xi_1\xi_3^4 + \xi_2\xi_3^4$	−0.2776953	−0.0017996
ξ_3	146.8181762	0.8989489	$\xi_1^3\xi_2^2 + \xi_1^2\xi_2^3$	−6.7076955	−0.0406266
$\xi_1^2 + \xi_2^2$	35.0713907	0.2142270	$\xi_1^3\xi_3^2 + \xi_2^3\xi_3^2$	−3.4685406	−0.0212396
ξ_3^2	39.7233542	0.2410479	$\xi_1^2\xi_3^3 + \xi_2^2\xi_3^3$	−3.1830347	−0.0197211
$\xi_1\xi_2$	−6.5382509	−0.0395175	$\xi_1^3\xi_2\xi_3 + \xi_1\xi_2^3\xi_3$	−0.9665177	−0.0056201
$\xi_2\xi_3 + \xi_1\xi_3$	9.3383797	0.0571994	$\xi_1\xi_2\xi_3^3$	6.4082684	0.0394177
$\xi_1^3 + \xi_2^3$	13.0621534	0.0804563	$\xi_1^2\xi_2^2\xi_3$	6.8313282	0.0421861
ξ_3^3	−71.3281314	−0.4334456	$\xi_1^2\xi_2\xi_3^2 + \xi_1\xi_2^2\xi_3^2$	5.3534545	0.0318521
$\xi_1^2\xi_2 + \xi_1\xi_2^2$	−44.9567002	−0.2750253	$\xi_1^6 + \xi_2^6$	−12.4644938	−0.0766375
$\xi_1^2\xi_3 + \xi_2^2\xi_3$	24.5380061	0.1507423	ξ_3^6	−0.6684773	−0.0038384
$\xi_1\xi_3^2 + \xi_2\xi_3^2$	1.8643311	0.0111332	$\xi_1^5\xi_2 + \xi_1\xi_2^5$	26.7119438	0.1643648
$\xi_1\xi_2\xi_3$	−29.3644926	−0.1808657	$\xi_1^5\xi_3 + \xi_2^5\xi_3$	−17.6882451	−0.1092554
$\xi_1^4 + \xi_2^4$	−4.8237103	−0.0299710	$\xi_1\xi_3^5 + \xi_2\xi_3^5$	−4.7721125	−0.0292397
ξ_3^4	−1.5597289	−0.0106946	$\xi_1^4\xi_2^2 + \xi_1^2\xi_2^4$	8.2409201	0.0517293
$\xi_1^3\xi_2 + \xi_1\xi_3^2$	−67.1009276	−0.4112046	$\xi_1^4\xi_3^2 + \xi_2^4\xi_3^2$	5.3515331	0.0329919
$\xi_1^3\xi_3 + \xi_2^3\xi_3$	20.4819674	0.1251849	$\xi_1^2\xi_3^4 + \xi_2^2\xi_3^4$	11.3069744	0.0691577
$\xi_1\xi_3^3 + \xi_2\xi_3^3$	−2.0317707	−0.0121537	$\xi_1^4\xi_2\xi_3 + \xi_1\xi_2^4\xi_3$	−15.7487383	−0.0959680
$\xi_1^2\xi_2^2$	−7.8689389	−0.0482565	$\xi_1\xi_2\xi_3^4$	6.1330762	0.0375566
$\xi_1^2\xi_3^2 + \xi_2^2\xi_3^2$	−7.2853015	−0.0440467	$\xi_1^3\xi_2^3$	7.3390310	0.0422062
$\xi_1^2\xi_2\xi_3 + \xi_1\xi_2^2\xi_3$	25.6389599	0.1569756	$\xi_1^3\xi_3^3 + \xi_2^3\xi_3^3$	5.2034233	0.0320124
$\xi_1\xi_2\xi_3^2$	−21.7148520	−0.1328672	$\xi_1^3\xi_2^2\xi_3 + \xi_1^2\xi_2^3\xi_3$	−27.2954011	−0.1677809
$\xi_1^5 + \xi_2^5$	−0.4104298	−0.0021155	$\xi_1^3\xi_2\xi_3^2 + \xi_1\xi_2^3\xi_3^2$	10.1070117	0.0615700
ξ_3^5	6.6263342	0.0400874	$\xi_1^2\xi_2\xi_3^3 + \xi_1\xi_2^2\xi_3^3$	−14.1857226	−0.0863394
$\xi_1^4\xi_2 + \xi_1\xi_2^4$	−9.8435987	−0.0609902	$\xi_1^2\xi_2^2\xi_3^2$	−12.0083242	−0.0740831
$(\chi^2)^{1/2} = 5.62 \times 10^{-6}$ E_h					

[a] All coefficients given in E_h

$$S_{ab} = \frac{\hbar\nu_{ab}}{c}\frac{N_A}{Q_v}\frac{1.012510\times10^6}{RT}B_{ba}e^{-hc\nu_{0a}/kT}\left(1-e^{-hc\nu_{ab}/kT}\right) \quad (7)$$

respectively, where Q_v is the vibrational partition function and ν_{ab} is the energy of the $|\Psi_b\rangle \leftarrow |\Psi_a\rangle$ transition. The probability of transition between two rovibrational states $|\Psi^{RV}{}_a\rangle$ and $|\Psi^{RV}{}_b\rangle$ were calculated using,

$$R_{ab}^2 = \sum_{m_a}\sum_{m_a}\left|\left\langle\Psi^{RV}_{v_a,J_aK_am_a}|\mu_{sf}|\Psi^{RV}_{v_b,J_bK_bm_b}\right\rangle\right|^2 \quad (8)$$

where μ_{sf} is the DMS transformed to the space-fixed frame of reference [34]. The associated rovibrational spectral intensity may then be calculated,

$$S_{ab}^2 = \frac{8\pi^3}{3hc}\frac{C_AN_A}{Q_VQ_R}\frac{g_{nsi}}{RT}\nu_{ab}\left[e^{-hcE_a/kT} - e^{-hcE_b/kT}\right]R_{ab}^2 \quad (9)$$

where C_A is the isotopic abundance, g_{nsi} is the nuclear statistical weight of the initial state and Q_R is the rotational partition function.

5 Results and discussion

5.1 Electronic structure of ($^1A_1$) NaH_2^+

Ab initio equilibrium parameters of ($^1A_1$) NaH_2^+ including bond lengths (R_e), $R_e(H_2)$, D_0, ω_1, ω_2 and ω_3 are collated in Table 1. The results of this work indicate that the minimum-energy structure of the ground state is of C_{2v} symmetry, in concurrence with previously reported data. Nevertheless, the CCSD(T) ansatz employed presently predicts an equilibrium structure disparate to those previous investigations in a quantitative sense. For example, the R_e value of this work is ca. 0.03–0.15 Å smaller than all previously reported HF and MP2 values, with the exception of the SCF MO result of Switalski et al. [10]. The latter ansatz employed a model core potential and yielded an R_e value of 2.38 Å. There is better agreement between the description of the H_2 moiety in the molecule. From Table 1 it is evident that HF ansatz [11, 12, 35] predicted $R_e(H_2)$ to be 0.732–0.740 Å, whereas MP2 methods [13, 15, 16]

yielded $R_e(H_2)$ to be 0.737–0.740 Å. The $R_e(H_2)$ value reported in this work is larger than all previous data by at least ca. 0.006 Å.

The data in Table 1 with respect to the harmonic fundamentals of ($^1A_1$) NaH_2^+ suggest that the $^1A_1$ PES is particularly sensitive with respect to the ab initio ansatz employed. This is particularly evident upon comparison of ω_2 fundamentals. This fundamental mode essentially corresponds to ω_e in the H_2 moiety. From Table 1, it can be seen that the CCSD(T) ω_2 value is generally 200–250 cm^{-1} smaller than previously reported HF values, and ca. 140 cm^{-1} smaller than the MP2/6-311G+(3*df*, 2*p*) value reported by Bushnell et al. [13]. For comparison, $\omega_e(H_2)$ calculated using CCSD/aug-cc-pVQZ is 4,399 cm^{-1}. This implies that the anisotropy of the Na^+–H_2 interaction is less pronounced than those of the Li^+–H_2 [5] and Mg^{2+}–H_2 [17] interactions. For these isovalent and isoelectronic series ω_2 were calculated to be 4,277 and 3,951 cm^{-1}, respectively, using equivalent CCSD(T) ansatz.

The [($^1A_1$) $NaH_2^+ \rightarrow$ ($^1S_0$) $Na^+ +$ ($^1\sum_g^+$) H_2 ($v = 0$)] dissociation energy has been measured experimentally by Bushnell et al. [13] to be 10.3 ± 0.8 kJ mol^{-1}. In this work, D_0 (NaH_2^+) has been evaluated to be 10.3 kJ mol^{-1} in excellent agreement with experiment [13]. The zero-point energy (ZPE) of ($^1A_1$) NaH_2^+ was computed here using an 8,000 term vibrational CI wave function in conjunction with the full CCSD(T) ($^1A_1$) NaH_2^+ PES (*vide infra*). Curtiss and Pople [12] previously reported D_0 to be 10.3 kJ mol^{-1} using HF/6-31G(*d*) (a fortuitous agreement). There is ca. 1 kJ mol^{-1} agreement between the MP2 D_0 values reported by Barbatti et al. [15] (MP2/6-311G(*d*, *p*)), Vitillo et al. [16] (MP2/6-311G+(3*df*, 2*p*)) and the CCSD(T) value of this work.

5.2 Potential energy surface

The discrete CCSD(T) PES of ($^1A_1$) NaH_2^+ was constructued using an iterative algorithm described elsewhere

Table 3 Power series expansion coefficients of the CCSD(T) dipole moment surface

μ_y						μ_x			
Term	Coefficient	Term	Coefficient	Term	Coefficient	Term	Coefficient	Term	Coefficient
a_{000}	−1.5923−01[a]	a_{204}	−3.8794−02	a_{400}	3.5102−03	b_{100}	1.1624−01	b_{312}	1.9049−01
a_{001}	−7.0854−02	a_{205}	−1.6528−01	a_{401}	1.8616−02	b_{101}	1.1742−03	b_{313}	1.4271−01
a_{002}	1.0434−02	a_{210}	−4.5935−02	a_{402}	−3.4477−02	b_{102}	9.3593−03	b_{320}	3.4777−02
a_{003}	3.0127−01	a_{211}	−1.2614−01	a_{403}	1.9968−02	b_{103}	1.3685−02	b_{321}	1.6272−01
a_{004}	−6.8754−01	a_{212}	2.1122−01	a_{410}	−8.4723−03	b_{104}	−5.9478−02	b_{322}	−2.6530−01
a_{005}	5.1555−03	a_{213}	−9.9924−03	a_{411}	2.9648−01	b_{105}	−1.2268+00	b_{400}	1.1346−01
a_{006}	1.1849−04	a_{214}	−1.9147−02	a_{412}	−3.8606−01	b_{106}	−7.4600−04	b_{401}	1.1352−01
a_{007}	−1.9193−02	a_{220}	2.4490−04	a_{420}	−4.5369−02	b_{200}	−8.1113−02	b_{402}	−1.1660−03
a_{100}	2.5798−02	a_{221}	9.8001−07	a_{421}	−6.2732−03	b_{201}	1.6622−01	b_{403}	−2.2919−05
a_{101}	1.7546−02	a_{222}	−2.2920−02	a_{430}	−7.3667−02	b_{202}	2.6520−02	b_{410}	−4.7396−03
a_{102}	6.0412−02	a_{223}	3.8669−02	a_{500}	7.5881−02	b_{203}	5.3227−02	b_{411}	−6.9036−03
a_{103}	9.2429−03	a_{300}	−1.5387−01	a_{501}	2.1999−02	b_{204}	−2.3108−01	b_{412}	8.1149−02
a_{104}	−7.7948−06	a_{301}	2.0967−01	a_{502}	9.3890−03	b_{205}	8.2696−05	b_{420}	−1.7516−01
a_{105}	−8.8886−02	a_{302}	−4.5396−02	a_{510}	−2.2692−02	b_{210}	8.7224−03	b_{421}	−4.0503−02
a_{106}	2.0615−01	a_{303}	5.6218−02	a_{511}	2.8154−04	b_{211}	8.6484−02	b_{430}	6.5253−02
a_{110}	−1.9161−01	a_{304}	2.3605−01	a_{520}	1.4148−03	b_{212}	−3.0505−01	b_{500}	−4.0742−02
a_{111}	5.7501−02	a_{310}	6.4118−02	a_{600}	−1.7784−05	b_{213}	1.0443+00	b_{501}	1.2486−01
a_{112}	8.9926−02	a_{311}	7.6925−02	a_{601}	−1.4397−05	b_{214}	−6.7185−01	b_{502}	3.3447−01
a_{113}	1.8006−02	a_{312}	−4.5988−03	a_{610}	−1.2306−08	b_{300}	−4.3077−01	b_{510}	2.1898−01
a_{114}	3.5375−02	a_{313}	2.1382−02	a_{700}	9.2517−10	b_{301}	−4.3239−01	b_{511}	1.7985−02
a_{115}	−3.1537−03	a_{320}	−4.8607−02			b_{302}	1.1973−01	b_{520}	1.5497−02
a_{200}	−6.5521−06	a_{321}	7.5411−04			b_{303}	1.1094−04	b_{600}	−2.0458−04
a_{201}	3.8694−02	a_{322}	1.2946−03			b_{304}	5.5261−02	b_{601}	−6.8587−05
a_{202}	−3.0885−02	a_{330}	−5.8087−06			b_{310}	−1.6819−01	b_{610}	−2.4287−05
a_{203}	1.4375−02	a_{331}	−5.0178−08			b_{311}	1.7038−01	b_{700}	2.4817−07
$(\chi^2)^{1/2} = 8.84 \times 10^{-3}$ a.u.						$(\chi^2)^{1/2} = 1.40 \times 10^{-3}$ a.u.			

All Coefficients given in a.u.

[a] −1.5923−01 denotes -1.5923×10^{-1}

[36, 37]. Briefly, the initial surface consisted of 34 points located along the diagonal t_1, t_2, t_3 components of the normal-coordinate domain. A preliminary diagonal analytical representation was constructed, from which a denser HEG quadrature grid was calculated. This grid consisted of 20 quadrature points in each t coordinate. The final discrete PES grid consisted of a 118-point subset of these 8,000 quadrature points.

The CCSD(T) PES was subsequently embedded in the molecular rovibrational Hamiltonian via a Padé approximant representation [38–42]. It was found that the most suitable analytical representation of the discrete CCSD(T) energy grid, both topologically and statistically, was a $P(6,6)$ expansion of the Ogilvie (OGL) expansion parameter ξ [43],

$$P(6,6) = \frac{\sum_{i,j,k=0}^{6} C_{ijk} \xi_1^i \xi_2^j \xi_3^k}{\sum_{i',j',k'=1}^{6} C_{i'j'k'} \xi_1^{i'} \xi_2^{j'} \xi_3^{k'}} \tag{10}$$

where,

$$\xi_i = \frac{2(R_i - R_i^e)}{R_i + R_i^e} \tag{11}$$

During the optimisation of the coefficients C_{ijk} and $C_{i'j'k'}$ the singular values $\sigma_{85-88,91-99}$ were eliminated using singular-value decomposition (SVD) [44]. The $P(6,6)$ analytical representation exhibited a residual error ($(\chi^2)^{1/2}$) value of 1.23 cm^{-1} with respect to the discrete CCSD(T) energy grid. Two-dimensional constant energy projections of the $P(6,6)$ CCSD(T) PES are given in Fig. 1, and the term coefficients C_{ijk} and $C_{i'j'k'}$ are listed in Table 2.

5.3 Dipole moment surface

A subset of 90 CCSD(T) PES geometries comprised the discrete DMS of ($^1A_1$) NaH_2^+. For all calculated dipole moments, the molecule was held in the Eckart frame. As

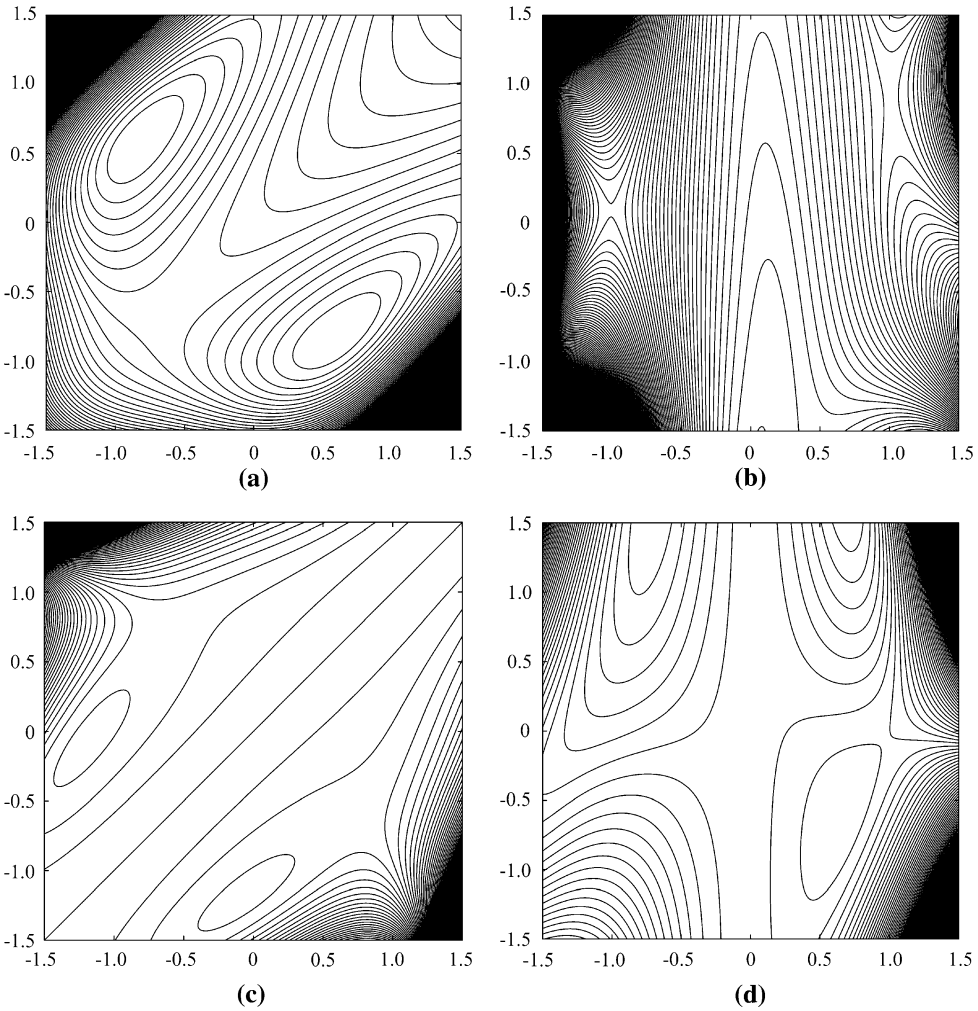

Fig. 2 Contour projections of the ($^1A_1$) NaH_2^+ CCSD(T) dipole moment surface in terms of internal-displacement coordinates (a.u.): **a** μ_y, ρ_1 (*horizontal axis*) vs. ρ_2 (*vertical axis*); **b** μ_y, ρ_3 (*horizontal axis*) vs. ρ_1 (*vertical axis*); **c** μ_x, ρ_1 (*horizontal axis*) vs. ρ_2 (*vertical axis*); and **d** μ_x, ρ_3 (*horizontal axis*) vs. ρ_1 (*vertical axis*). Contours spaced at: **a** 0.058; **b** 0.013; **c** 0.051; and **d** 0.105 (a.u.)

such, the centre of mass was necessarily coincident with the origin of the Cartesian coordinate space, and the molecular dipole moment was described completely by the x and y components. The discrete CCSD(T) DMS of ($^1A_1$) NaH_2^+ was embedded in the molecular rovibrational Hamiltonian in the manner of Gabriel et al. [45]. In particular, μ_x and μ_y were constructed analytically using power-series expansions of internal displacement coordinates ρ_1, ρ_2 and ρ_3. The most topologically and statistically optimal representations of μ_x and μ_y were 7th order expansions,

$$\mu_x(\rho_1,\rho_2,\rho_3) = \sum_{i,j,k=0}^{7} b_{ijk}\rho_1^i\rho_2^j\rho_3^k \tag{12}$$

and

$$\mu_y(\rho_1,\rho_2,\rho_3) = \sum_{i,j,k=0}^{7} a_{ijk}\rho_1^i\rho_2^j\rho_3^k \tag{13}$$

The analytical μ_x and μ_y functions were therefore described by 50 b_{ijk} and 70 a_{ijk} coefficients, respectively.

Table 4 Structural properties of low-lying vibrational states of ($^1A_1$) NaH_2^+, ($^1A'$) $NaHD^+$ and ($^1A_1$) NaD_2^+

i	VBO (cm^{-1})	Assign $\|t_1t_2t_3\rangle$	Sym.	Weight[a]	$\langle R\rangle$(Na–H)(Å)	$\langle R\rangle$(Na–D) (Å)	θ (°)
($^1A_1$) NaH_2^+							
0	0.00[b]	$\|000\rangle$	a_1	0.88	2.4995		17.1
1	341.02	$\|100\rangle$	a_1	0.71	2.5625		16.8
2	646.02	$\|001\rangle$	b_2	0.82	2.4769		16.1
3	705.75	$\|200\rangle$	a_1	0.52	2.5908		16.7
4	1,057.75	$\|101\rangle$	b_2	0.73	2.5227		16.0
5	1,096.90	$\|200\rangle$, $\|300\rangle$	a_1	0.56,0.36	2.6113		16.7
6	1,428.86	$\|002\rangle$	a_1	0.72	2.4327		15.9
7	1,484.30	$\|201\rangle$	b_2	0.63	2.5544		16.0
8	1,508.92	$\|300\rangle$, $\|600\rangle$	a_1	0.56,0.35	2.6308		16.7
9	1,905.83	$\|102\rangle$	a_1	0.68	2.4839		15.8
($^1A'$) $NaHD^+$							
0	0.00[c]	$\|000\rangle$	a'	0.87	2.4987	2.4990	17.0
1	264.68	$\|100\rangle$	a'	0.67	2.5578	2.5595	16.7
2	530.18	$\|001\rangle$	a''	0.59	2.5271	2.5522	16.3
3	558.21	$\|200\rangle$, $\|400\rangle$	a'	0.31, 0.24	2.5522	2.5336	16.4
4	827.25	$\|101\rangle$, $\|301\rangle$	a''	0.46, 0.18	2.5617	2.5845	16.3
5	871.88	$\|101\rangle$, $\|001\rangle$	a''	0.44, 0.20	2.5777	2.5450	16.3
6	1,134.31	$\|201\rangle$, $\|101\rangle$	a''	0.39, 0.17	2.5526	2.5825	16.1
7	1,178.21	$\|002\rangle$, $\|600\rangle$	a'	0.44, 0.20	2.5563	2.5547	16.1
8	1,223.73	$\|002\rangle$, $\|012\rangle$	a'	0.42, 0.22	2.5221	2.5094	16.0
9	1,461.74	$\|301\rangle$, $\|501\rangle$	a''	0.30, 0.24	2.5745	2.6004	16.1
($^1A_1$) NaH_2^+							
0	0.00[d]	$\|000\rangle$	a_1	0.87		2.4976	17.0
1	229.45	$\|100\rangle$	a_1	0.64		2.5680	16.6
2	405.22	$\|001\rangle$	b_2	0.77		2.5000	16.0
3	464.58	$\|100\rangle$, $\|200\rangle$	a_1	0.54, 0.38		2.6056	16.5
4	669.84	$\|101\rangle$	b_2	0.61		2.5446	15.9
5	715.04	$\|200\rangle$	a_1	0.60		2.6246	16.4
6	869.49	$\|002\rangle$	a_1	0.65		2.4720	15.6
7	942.24	$\|101\rangle$, $\|201\rangle$	b_2	0.48, 0.44		2.5741	15.9
8	980.94	$\|300\rangle$	a_1	0.55		2.6392	16.4
9	1,176.36	$\|102\rangle$	a_1	0.58		2.5108	15.6

[a] See Eq. 2

[b] ($^1A_1$) NaH_2^+ zero-point energy = 2,561.44 cm^{-1}

[c] ($^1A'$) $NaHD^+$ zero-point energy = 2,213.73 cm^{-1}

[d] ($^1A_1$) NaH_2^+ zero-point energy = 1,814.24 cm^{-1}

These coefficients are defined in Table 3. Two-dimensional projections of μ_x and μ_y are presented in Fig. 2, from which it is observed that physically acceptable representations of the CCSD(T) dipole moment grid were obtained without the use of SVD in the optimisation of the coefficients b_{ijk}, a_{ijk}.

5.4 Vibrational and rovibrational states of NaH_2^+, $NaHD^+$ and NaD_2^+

The low-lying vibrational band origins (VBOs) of ($^1A_1$) NaH_2^+ are detailed in Table 4, as are the respective assignments and vibration-averaged structures. Each state listed here has been assigned using a single dominant configuration, excepting the states with VBOs at 1,096.90 and 1,508.92 cm^{-1}. These latter vibrational state are predominantly composed of the ($|200\rangle$, $|300\rangle$) and ($|300\rangle$, $|600\rangle$) configurations, respectively. For the fundamental $|100\rangle$ and $|001\rangle$ modes, configuration mixing in the vibrational wave function is limited. For example, the weights of the $|100\rangle$ and $|001\rangle$ terms in these states are 0.71 and 0.82, respectively. Similarly, the $|010\rangle$ term in the a_2 bend fundamental (with VBO at 4,114.22 cm^{-1}) exhibited a configuration weight of 0.77. There is more configuration mixing in the low-lying overtone bands, as expected. For instance, the a_1 with VBOs at 705.75 and 1,508.82 cm^{-1} correspond to the $|200\rangle$ and $|300\rangle$ bands, respectively. These states are more delocalised, with the predominant terms having configuration weights of 0.52 and 0.56, respectively.

Extensive configuration mixing is observed for the low-lying vibrational states of ($^1A'$) $NaHD^+$, which are presented in Table 4. For example, only the ground state and the $|100\rangle$ and $|001\rangle$ fundamental modes have been assigned using a single dominant term. The weights of the primary configurations in the latter two states are 0.67 and 0.59, respectively, suggesting that a greater degree of delocalisation is present

Table 5 Ab initio rovibrational transition wavenumbers (cm^{-1}) and intensities (cm $molecule^{-1}$) of NaH_2^+ in the H–H stretch band for $J \leq 5$ and $K \leq 2$

R Branch			*P* Branch			*Q* Branch		
Transition	v_{ab}	S_{ab}	Transition	v_{ab}^a	S_{ab}	Transition	v_{ab}^a	S_{ab}
$K = 0$								
$1^a_{0,1} \leftarrow 0_{0,0}$	4,117.28	4.59−33[b]	$0_{0,0} \leftarrow 1_{0,1}$	4,111.23	5.80−35			
$2_{0,2} \leftarrow 1_{0,1}$	4,120.41	1.78−30	$1_{0,1} \leftarrow 2_{0,2}$	4,108.32	1.93−33			
$3_{0,3} \leftarrow 2_{0,2}$	4,123.62	1.02−32	$2_{0,2} \leftarrow 3_{0,3}$	4,105.49	7.45−33			
$4_{0,4} \leftarrow 3_{0,3}$	4,126.92	8.80−33	$3_{0,3} \leftarrow 4_{0,4}$	4,102.75	6.25−33			
$5_{0,5} \leftarrow 4_{0,4}$	4,130.31	1.03−30	$4_{0,4} \leftarrow 5_{0,5}$	4,100.12	4.72−33			
$K = 1$								
$2_{1,2} \leftarrow 1_{1,1}$	4,117.69	2.71−31	$1_{1,0} \leftarrow 2_{1,1}$	4,105.58	6.86−34	$1_{1,1} \leftarrow 1_{1,0}$	4,111.54	2.37−31
$2_{1,1} \leftarrow 1_{1,0}$	4,117.80	2.38−32	$1_{1,1} \leftarrow 2_{1,2}$	4,105.68	2.66−31	$1_{1,0} \leftarrow 1_{1,1}$	4,111.64	1.04−31
$3_{1,3} \leftarrow 2_{1,2}$	4,120.94	2.90−31	$2_{1,1} \leftarrow 3_{1,2}$	4,102.79	5.92−32	$2_{1,2} \leftarrow 2_{1,1}$	4,111.64	2.27−30
$3_{1,2} \leftarrow 2_{1,1}$	4,121.11	2.19−32	$2_{1,2} \leftarrow 3_{1,3}$	4,102.93	1.22−31	$2_{1,1} \leftarrow 2_{1,2}$	4,111.94	2.24−32
$4_{1,4} \leftarrow 3_{1,3}$	4,124.30	1.03−33	$3_{1,2} \leftarrow 4_{1,3}$	4,100.11	1.15−32	$3_{1,3} \leftarrow 3_{1,2}$	4,111.79	6.86−31
$4_{1,3} \leftarrow 3_{1,2}$	4,124.53	1.48−34	$3_{1,3} \leftarrow 4_{1,4}$	4,100.29	7.83−32	$3_{1,2} \leftarrow 3_{1,3}$	4,112.40	2.57−32
$5_{1,5} \leftarrow 4_{1,4}$	4,127.78	5.21−32	$4_{1,3} \leftarrow 5_{1,4}$	4,097.56	1.48−32	$4_{1,4} \leftarrow 4_{1,3}$	4,112.02	1.57−33
$5_{1,4} \leftarrow 4_{1,3}$	4,128.07	5.83−30	$4_{1,4} \leftarrow 5_{1,5}$	4,097.78	4.92−34	$4_{1,3} \leftarrow 4_{1,4}$	4,112.53	2.69−31
						$5_{1,5} \leftarrow 5_{1,4}$	4,112.33	5.04−32
						$5_{1,4} \leftarrow 5_{1,5}$	4,113.83	3.59−30
$K = 2$								
$3_{2,2} \leftarrow 2_{2,1}$	4,128.13	1.01−32	$2_{2,0} \leftarrow 3_{2,1}$	4,109.41	9.17−33	$2_{2,1} \leftarrow 2_{2,0}$	4,118.28	5.78−33
$3_{2,1} \leftarrow 2_{2,0}$	4,128.13	1.08−30	$2_{2,1} \leftarrow 3_{2,2}$	4,109.41	1.38−34	$2_{2,0} \leftarrow 2_{2,1}$	4,118.28	2.13−32
$4_{2,3} \leftarrow 3_{2,1}$	4,132.35	2.02−32	$3_{2,1} \leftarrow 4_{2,2}$	4,107.44	1.22−30	$3_{2,2} \leftarrow 3_{2,1}$	4,119.26	2.01−34
$4_{2,2} \leftarrow 3_{2,2}$	4,132.35	7.44−34	$3_{2,2} \leftarrow 4_{2,3}$	4,107.44	8.37−32	$3_{2,1} \leftarrow 3_{2,2}$	4,119.26	4.44−31
$5_{2,4} \leftarrow 4_{2,3}$	4,136.93	1.25−31	$4_{2,2} \leftarrow 5_{2,3}$	4,105.78	8.66−32	$4_{2,3} \leftarrow 4_{2,2}$	4,120.54	2.22−34
$5_{2,3} \leftarrow 4_{2,2}$	4,136.93	3.29−33	$4_{2,3} \leftarrow 5_{2,4}$	4,105.78	7.00−32	$4_{2,2} \leftarrow 4_{2,3}$	4,120.54	1.89−32
						$5_{2,4} \leftarrow 5_{2,3}$	4,122.17	1.41−32
						$5_{2,3} \leftarrow 5_{2,4}$	4,122.18	3.08−33

[a] All transitions given in terms of J_{K_a,K_c}, see reference [9]

[b] 4.59−33 denotes 4.59×10^{-33}

in the vibrational wave function of (^{1}A′) $NaHD^+$ than those of ($^1A_1$) NaH_2^+ and ($^1A_1$) NaD_2^+. The characters of all other vibrational states listed in Table 4 are more multi-configurational in nature, and have been described using two dominant configurations.

The lowest 10 VBOs, their respective assignments and vibration-averaged structures of ($^1A_1$) NaD_2^+ are given in Table 4. Each of the lowest 10 states has been assigned using a single dominant configuration, except for the a_1 and b_2 states corresponding to the VBOs at 464.58 and 942.24 cm^{-1}, respectively. The latter vibrational states were found to be composed primarily from $(0.54 \times |100\rangle + 0.38 \times |200\rangle)$ and $(0.48 \times |101\rangle + 0.44 \times |201\rangle)$ terms, respectively. As for ($^1A_1$) NaH_2^+, the fundamental vibrational states of ($^1A_1$) NaH_2^+ have been assigned most definitively. For example, the fundamental a_1 breathe and b_2 asymmetric stretch modes include $|100\rangle$ and $|001\rangle$ configuration weights of 0.64 and 0.77, respectively. These vibrational states are therefore more delocalised than the analogous states for ($^1A_1$) NaH_2^+. The vibrational overtone bands for ($^1A_1$) NaH_2^+ also possess more multi-configurational character than the fundamental states. For example, the $|002\rangle$ term exhibits a configuration weight of 0.65 in the lowest b_2 asymmetric stretch overtone (VBO = 869.49 cm^{-1}). Similarly, the second overtone in the a_1 breathe mode includes the $|300\rangle$ term with a configuration weight of 0.55.

All rovibrational states of ($^1A_1$) NaH_2^+, (^{1}A′) $NaHD^+$ and ($^1A_1$) NaD_2^+ for $v \leq 10$, $J \leq 5$ have been calculated in this work. Rotational constant (**A**, **B**, **C**, **D**) and Coriolis coupling (**F**) matrix elements spanned zby the lowest ten vibrational states of each species have also been evaluated. These data are available from the authors upon request. The κ asymmetry parameters for the ground vibrational states of ($^1A_1$) NaH_2^+, (^{1}A′) $NaHD^+$ and ($^1A_1$) NaH_2^+ have been calculated to be −0.9516, −0.9497 and −0.9473, respectively. As such, each species is a near-prolate top. All rovibrational states have been assigned using the Mulliken J, K_a, K_c assignment scheme [9].

5.5 Vibration-averaged structures of NaH_2^+, $NaHD^+$ and NaD_2^+

The effects of vibration-averaging on the equilibrium Na–H bond length is quite noticeable in the vibrational ground state of ($^1A_1$) NaH_2^+. Comparison of data from Tables 1

Table 6 Comparison of experimental and ab initio rovibrational transition wavenumbers (cm^{-1}) of LiH_2^+ [a] for $J \leq 5$ and $K \leq 2$

R Branch				*P* Branch			
Transition	Exp.	Theor.	Δ	Transition	Exp.	Theor.	Δ
$K = 0$							
$1_{0,1} \leftarrow 0_{0,0}$	4,058.34	4,063.97	5.64	$0_{0,0} \leftarrow 1_{0,1}$		4,053.86	
$2_{0,2} \leftarrow 1_{0,1}$	4,063.26	4,069.10	5.84	$1_{0,1} \leftarrow 2_{0,2}$	4,043.37	4,048.87	5.50
$3_{0,3} \leftarrow 2_{0,2}$	4,068.15	4,074.26	6.11	$2_{0,2} \leftarrow 3_{0,3}$	4,038.36	4,043.95	5.58
$4_{0,4} \leftarrow 3_{0,3}$	4,072.99	4,079.45	6.46	$3_{0,3} \leftarrow 4_{0,4}$	4,033.34	4,039.09	5.75
$5_{0,5} \leftarrow 4_{0,4}$	4,077.79	4,084.67	6.88	$4_{0,4} \leftarrow 5_{0,5}$	4,028.35	4,034.31	5.96
$K = 1$							
$2_{1,2} \leftarrow 1_{1,1}$	4,059.07	4,064.55	5.48	$1_{1,0} \leftarrow 2_{1,1}$	4,039.24	4,044.36	5.12
$2_{1,1} \leftarrow 1_{1,0}$	4,059.38	4,064.83	5.44	$1_{1,1} \leftarrow 2_{1,2}$	4,039.54	4,044.64	5.10
$3_{1,3} \leftarrow 2_{1,2}$	4,063.88	4,069.64	5.76	$2_{1,1} \leftarrow 3_{1,2}$	4,034.16	4,039.38	5.22
$3_{1,2} \leftarrow 2_{1,1}$	4,064.34	4,070.05	5.71	$2_{1,2} \leftarrow 3_{1,3}$	4,034.62	4,039.80	5.18
$4_{1,4} \leftarrow 3_{1,3}$	4,068.64	4,074.76	6.12	$3_{1,2} \leftarrow 4_{1,3}$	4,029.11	4,034.48	5.37
$4_{1,3} \leftarrow 3_{1,2}$	4,069.26	4,075.31	6.05	$3_{1,3} \leftarrow 4_{1,4}$	4,029.68	4,035.03	5.35
$5_{1,5} \leftarrow 4_{1,4}$	4,073.37	4,079.92	6.56	$4_{1,3} \leftarrow 5_{1,4}$	4,024.03	4,029.65	5.62
$5_{1,4} \leftarrow 4_{1,3}$	4,074.12	4,080.60	6.48	$4_{1,4} \leftarrow 5_{1,5}$	4,024.77	4,030.34	5.57
$K = 2$							
$3_{2,2} \leftarrow 2_{2,1}$	4,052.79	4,057.95	5.15	$2_{2,0} \leftarrow 3_{2,1}$	4,023.24	4,027.83	4.59
$3_{2,1} \leftarrow 2_{2,0}$	4,052.79	4,057.95	5.16	$2_{2,1} \leftarrow 3_{2,2}$	4,023.24	4,027.83	4.59
$4_{2,3} \leftarrow 3_{2,1}$	4,057.60	4,063.20	5.60	$3_{2,1} \leftarrow 4_{2,2}$	4,018.25	4,023.09	4.84
$4_{2,2} \leftarrow 3_{2,2}$	4,057.60	4,063.20	5.60	$3_{2,2} \leftarrow 4_{2,3}$	4,018.25	4,023.09	4.84
$5_{2,4} \leftarrow 4_{2,3}$	4,062.38	4,068.51	6.12	$4_{2,2} \leftarrow 5_{2,3}$	4,013.35	4,018.46	5.11
$5_{2,3} \leftarrow 4_{2,2}$	4,062.38	4,068.51	6.13	$4_{2,3} \leftarrow 5_{2,4}$	4,013.35	4,018.46	5.11

[a] Experimental data from reference [8]. All transitions given in terms of J_{K_a,K_c}, see reference [9]

Table 7 Radiative properties of low-lying vibrational states of ($^1A_1$) NaH_2^+, ($^1A'$) $NaHD^+$ and ($^1A_1$) NaD_2^+

i	VBO (cm^{-1})	μ^2 (a.u.^{2})	A_{0i} (s^{-1})	B_{0i} ($10^{-16}cm^3erg^{-1}$ s^2)	S_{0i} (cm $molecule^{-1}$)	τ (s)
($^1A_1$) NaH_2^+						
1	341.02	3.38+04[a]	4.20+05	6.36+06	3.07−12	6.13−07
2	646.02	3.06+04	2.59+06	5.76+06	6.24−12	3.29−07
3	705.75	1.26+04	1.39+06	2.38+06	2.84−12	1.56−07
4	1,057.75	1.41+04	5.22+06	2.65+06	4.88−12	5.54−08
5	1,096.90	6.96+02	2.88+05	1.31+05	2.50−13	5.64−08
6	1,428.86	9.35+02	8.55+05	1.76+05	4.40−13	1.86−07
7	1,484.30	8.95+03	9.18+06	1.69+06	4.38−12	1.52−08
8	1,508.92	7.15+00	7.71+03	1.35+03	3.56−15	2.64−08
9	1,905.83	2.04+03	4.43+06	3.84+05	1.28−12	1.75−08
($^1A'$) $NaHD^+$						
1	264.68	2.71+04	1.58+05	5.11+06	1.50−12	8.87−07
2	530.18	1.95+04	9.11+05	3.67+06	2.75−12	3.67−07
3	558.21	1.53+04	8.33+05	2.88+06	2.30−12	3.81−07
4	827.25	3.20+03	5.69+05	6.03+05	7.50−13	1.24−07
5	871.88	6.46+03	1.34+06	1.22+06	1.60−12	1.13−07
6	1,134.31	4.37+03	2.00+06	8.23+05	1.42−12	5.13−08
7	1,178.21	3.38+03	1.73+06	6.36+05	1.14−12	5.96−08
8	1,223.73	1.09+03	6.25+05	2.05+05	3.83−13	6.49−08
9	1,461.74	1.29+03	1.27+06	2.44+05	5.45−13	2.32−08
($^1A'$) $NaHD^+$						
1	229.45	2.68+04	1.02+05	5.05+06	1.04−12	1.05−06
2	405.22	1.53+04	3.18+05	2.87+06	1.34−12	1.42−06
3	464.58	9.02+03	2.84+05	1.70+06	9.44−13	3.80−07
4	669.84	8.17+03	7.70+05	1.54+06	1.32−12	2.70−07
5	715.04	2.61+02	2.99+04	4.91+04	4.54−14	2.00−07
6	869.49	1.56+03	3.22+05	2.94+05	3.36−13	7.20−07
7	942.24	5.01+03	1.31+06	9.43+05	1.17−12	8.00−08
8	980.94	4.52−01	1.34+02	8.51+01	1.10−16	1.10−07
9	1,176.36	1.56+03	7.94+05	2.93+05	4.58−13	8.01−08

[a] 3.38+04 denotes 3.38×10^4

and 4 indicate the $\langle R \rangle$ is ca. 0.1 Å larger than R_e, which corresponds to the PES minimum. The change in the H–Na–H bond angle is more tempered, with $\langle \theta \rangle$ being 0.7° smaller than the equilibrium value (θ_e). For the a_1 breathe and b_2 asymmetric stretch fundamental modes, the $\langle R \rangle$ values were calculated to be 2.5625 and 2.4769 Å, thus deviating from the ground state values by 0.0630 and −0.0226 Å, respectively. Contractions in $\langle \theta \rangle$ of 0.3 and 1.0° are also observed for the $|100\rangle$, $|001\rangle$ states, respectively. This illustrates the effects of configuration interaction in the vibrational wave function on observable quantities. These data cumulatively suggest that the analytical ($^1A_1$) NaH_2^+ PES exhibits a relatively small curvature in the immediate neighbourhood of the PES minimum. Comparison of the anharmonic and harmonic fundamental wavenumbers also assists in such a conclusion. For example, the $|100\rangle$, $|001\rangle$ and $|010\rangle$ VBOs differ from the CCSD(T) ω_1, ω_2 and ω_3 values by −9.3, −202.8 and 77.6 cm^{-1}, respectively. The exaggerated difference in the fundamental a_1 bend mode is typical of MH_2^{n+} species [5, 17, 18] and illustrates the high anharmonicity present in the a_1 breathe 1D PES coordinate. Vibration-averaged structures of ($^1A'$) $NaHD^+$ are also indicative of a flat PES in the region of the minimum. For $\langle R \rangle$(Na–H) and $\langle R \rangle$(Na–D), a difference of 0.0003 Å is observed for the ground vibrational state. For comparison, the same differences for ($^1A'$) $LiHD^+$ and ($^1A'$) $MgHD^+$ have been calculated to be 0.004 and 0.0783 Å [5, 17]. For the ground vibrational state of ($^1A_1$) NaD_2^+, isotopic substitution results in a contraction of 0.0014 Å in the $\langle R \rangle$(Na–D) value, compared to ($^1A'$) $NaHD^+$, as expected. The effect of this isotopic substitution is negligible with respect to $\langle \theta \rangle$.

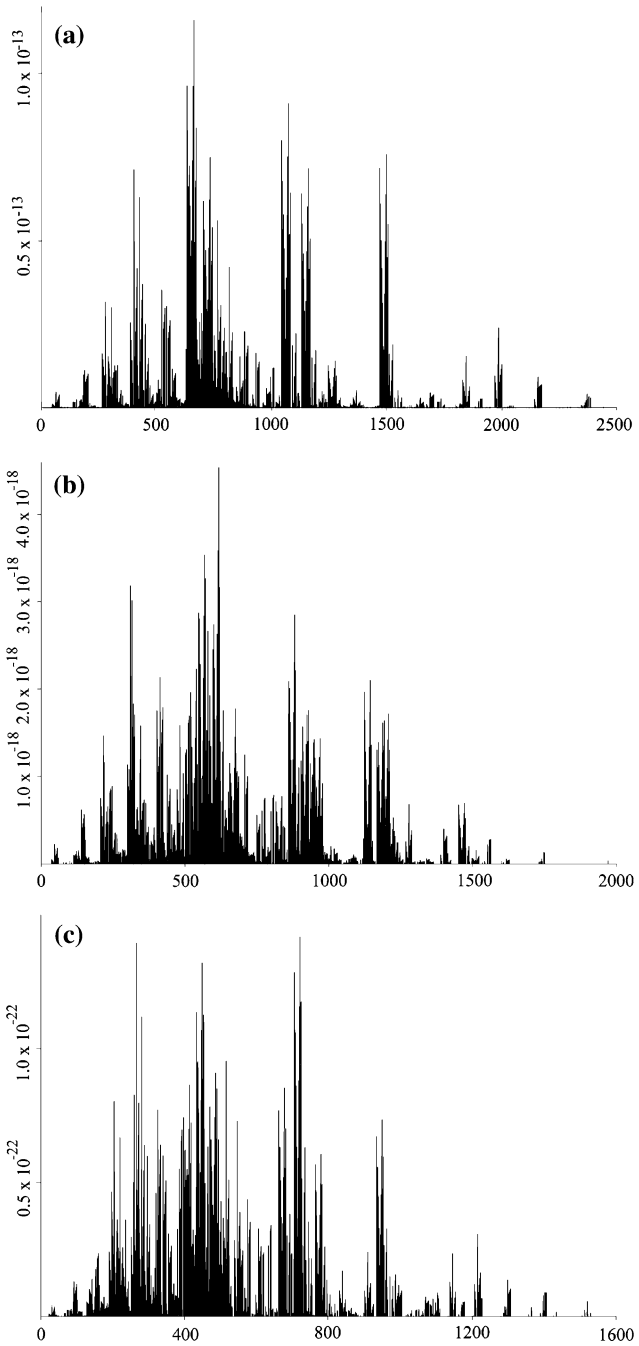

Fig. 3 Ab initio rovibrational spectra for $v \leq 10$, $J \leq 5$ and an intesity threshold S_{ab} at 296 K: **a** ($^1A_1$) NaH_2^+ ($S_{ab} = 1 \times 10^{-20}$), 7,764 lines, **b** ($^1A'$) NaH_2^+ ($S_{ab} = 1 \times 10^{-20}$), 4,855 lines; and **c** ($^1A_1$) NaH_2^+ ($S_{ab} = 1 \times 10^{-25}$), 4,162 lines. Transition wavenumbers and intensities given in cm^{-1} and cm $molecule^{-1}$, respectively

5.6 Comparison of the rovibrational structures of the NaH_2^+ and LiH_2^+ $v_{HH} = 1 \leftarrow v_{HH} = 0$ transitions

The wavenumbers and spectral intensities of low-lying rovibrational transitions ($J \leq 5$, $K \leq 2$) in the R, P and Q branches of the NaH_2^+ $v_{HH} = 1 \leftarrow v_{HH} = 0$ band are listed in Table 5. This transition corresponds to the VBO at 4,114.22 cm^{-1} and as such is close in energy to the same vibrational transition of the isovalent species LiH_2^+. The latter transition has been observed experimentally at 4,053.4 cm^{-1} [17]. A comparison of these experimental transition wavenumbers with theoretical values is made in Table 6. The latter were calculated using the algorithms of this work in conjunction with the ($^1A_1$) LiH_2^+ FCI PES of Page and von Nagy-Felsobuki [5]. It is evident from Table 6 that these experimental and theoretical transition wavenumbers of LiH_2^+ agree to within 5–6 cm^{-1} (ca. 0.1%) for $J \leq 5$ and $K \leq 2$. Similar relative errors were reported for the D–D stretch band of LiD_2^+ [5].

The differences in the vibrational red shifts of the respective $v_{HH} = 1 \leftarrow v_{HH} = 0$ bands for LiH_2^+ and NaH_2^+ are indicative of the relative effects of the metal ion charge distribution on the ground and first excited vibrational states of the H_2 moiety. In particular, the vibrational red shifts of these species may be interpreted as the differences in binding energies between the M^+-H_2 ($v_{HH} = 1$) and M^+-H_2 ($v_{HH} = 0$) complexes [7]. As such, the relative anisotropies of the Na^+-H_2 and Li^+-H_2 interactions may ultimately be compared. For example, the experimental band centre of the LiH_2^+ $v_{HH} = 1 \leftarrow v_{HH} = 0$ transition represents a red shift of 107.8 cm^{-1} relative to the $Q_1(0)$ transition of H_2 [46]. Similarly, the calculated band centre for the NaH_2^+ $v_{HH} = 1 \leftarrow v_{HH} = 0$ transition corresponds to a red shift of 47.0 cm^{-1} relative to the $Q_1(0)$ transition of H_2. Therefore, the potential surface of the Na^+-H_2 ($v_{HH} = 1$) complex is effectively 47.0 cm^{-1} deeper than that of the Na^+-H_2 ($v_{HH} = 0$) complex. This is in agreement with the known increases in the quadrupole moment/polarisability of H_2 in the first excited vibrational state [47]. Moreover, this trend is consistent with that observed experimentally for LiH_2^+ [7].

5.7 Vibrational and rovibrational spectra of NaH_2^+, $NaHD^+$ and NaD_2^+

Vibrational radiative properties, including vibration transition moments, Einstein A and B coefficients, vibration band strengths and radiative lifetimes have been calculated for the low-lying vibrational states of ($^1A_1$) NaH_2^+, ($^1A'$) $NaHD^+$ and ($^1A_1$) NaH_2^+. These data are given in Table 7. It is evident from this table that the $|001\rangle$ states of ($^1A_1$) NaH_2^+, ($^1A'$) $NaHD^+$ and ($^1A_1$) NaD_2^+ are of the greatest intensity, exhibiting S_{20} values of 6.24×10^{-12}, 2.75×10^{-12} and 1.34×10^{-12} cm $molecule^{-1}$, respectively. It is therefore anticipated that these bands would be dominant in the simulated ab initio rovibrational spectra of these species, given in Fig. 3 for $v \leq 10$ and $J \leq 5$. The rovibrational spectrum of ($^1A_1$) NaH_2^+ features several bands of similar intensity in the region 500–1,750 cm^{-1}.

Table 8 Assignments of prominent transitions in the ab initio rovibrational spectra of ($^1A_1$) NaH_2^+, ($^1A'$) $NaHD^+$ and ($^1A_1$) NaD_2^+

Initial					Final				Wavenumber (cm^{-1})	Intensity (cm $molecule^{-1}$)
$\|t_1t_2t_3\rangle$	J^a	K_a^a	K_c^a		$\|t_1t_2t_3\rangle$	J^a	K_a^a	K_c^a		
($^1A_1$) NaH_2^+										
$\|001\rangle$	5	0	5	←	$\|000\rangle$	4	0	4	661.89	1.16−13[b]
$\|001\rangle$	4	0	4	←	$\|000\rangle$	5	0	5	631.79	9.62−14
$\|001\rangle$	4	0	4	←	$\|000\rangle$	3	0	3	658.59	9.62−14
$\|101\rangle$	5	0	5	←	$\|000\rangle$	4	0	4	1,072.75	9.09−14
$\|001\rangle$	5	1	4	←	$\|000\rangle$	4	1	3	672.28	8.36−14
$\|001\rangle$	3	0	3	←	$\|000\rangle$	4	0	4	634.49	8.29−14
$\|001\rangle$	5	1	5	←	$\|000\rangle$	4	1	4	671.87	8.08−14
$\|101\rangle$	4	0	4	←	$\|000\rangle$	5	0	5	1,042.94	7.99−14
$\|201\rangle$	5	0	5	←	$\|000\rangle$	4	0	4	1,498.98	7.57−14
$\|101\rangle$	4	0	4	←	$\|000\rangle$	3	0	3	1,069.74	7.51−14
($^1A'$) $NaHD^+$										
$\|101\rangle$, $\|001\rangle$	5	0	5	←	$\|100\rangle$	4	0	4	617.43	4.54−18
$\|101\rangle$, $\|001\rangle$	4	0	4	←	$\|100\rangle$	3	0	3	615.37	3.59−18
$\|001\rangle$	5	0	5	←	$\|000\rangle$	4	0	4	568.10	3.54−18
$\|001\rangle$	5	1	4	←	$\|000\rangle$	4	1	3	571.19	3.27−18
$\|001\rangle$	5	1	5	←	$\|000\rangle$	4	1	4	570.99	3.22−18
$\|100\rangle$	5	1	4	←	$\|000\rangle$	5	0	5	310.65	3.18−18
$\|101\rangle$, $\|001\rangle$	5	1	4	←	$\|100\rangle$	4	1	3	620.69	3.16−18
$\|101\rangle$, $\|001\rangle$	5	1	5	←	$\|100\rangle$	4	1	4	620.50	3.11−18
$\|001\rangle$	5	1	4	←	$\|100\rangle$	5	0	5	316.19	3.02−18
$\|001\rangle$	4	0	4	←	$\|000\rangle$	5	0	5	547.63	2.87−18
($^1A_1$) NaH_2^+										
$\|101\rangle$, $\|201\rangle$	5	0	5	←	$\|100\rangle$	4	0	4	720.80	1.42−22
$\|100\rangle$	5	1	4	←	$\|000\rangle$	5	0	5	265.32	1.39−22
$\|101\rangle$	5	0	5	←	$\|100\rangle$	4	0	4	448.59	1.32−22
$\|101\rangle$, $\|201\rangle$	4	0	4	←	$\|100\rangle$	5	0	5	705.23	1.28−22
$\|101\rangle$, $\|201\rangle$	5	1	5	←	$\|100\rangle$	4	1	4	724.09	1.18−22
$\|100\rangle$, $\|200\rangle$	4	1	3	←	$\|100\rangle$	4	0	4	265.38	1.17−22
$\|101\rangle$, $\|201\rangle$	5	1	4	←	$\|100\rangle$	4	1	3	724.36	1.16−22
$\|101\rangle$, $\|201\rangle$	4	0	4	←	$\|100\rangle$	3	0	3	719.15	1.16−22
$\|101\rangle$	4	0	4	←	$\|100\rangle$	5	0	5	432.97	1.14−22
$\|101\rangle$	5	1	5	←	$\|100\rangle$	4	1	4	452.53	1.13−22

[a] See reference [9]

[b] 1.16−13 denotes 1.16×10^{-13}

The most intense transitions however have been assigned to the ($|001\rangle \leftarrow |000\rangle$) (∼650−750 cm^{-1}), ($|101\rangle \leftarrow |000\rangle$) (∼1,000−1,100 cm^{-1}) and ($|201\rangle \leftarrow |000\rangle$) (∼1,450−1,550 cm^{-1}) bands. Assignments of the most prominent transitions are given explicitly in Table 8. The rovibrational spectrum of ($^1A'$) $NaHD^+$ exhibits two predominant bands located at ∼550–650 cm^{-1} and ∼300–400 cm^{-1}. The most intense lines have been also characterised in Table 8. These transitions have been assigned to the ($|101\rangle$, $|001\rangle \leftarrow |100\rangle$) and ($|001\rangle \leftarrow |000\rangle$) bands, respectively. The rovibrational spectrum of ($^1A_1$) NaD_2^+ is dominated by three bands of intensity ca. 1.5×10^{-22} in the 300–500 cm^{-1} region. Nevertheless, the most intense transitions have been assigned unequivocally. In particular, transitions from the ($|100\rangle \leftarrow |000\rangle$) (∼250−350 cm^{-1}), ($|001\rangle$, $|201\rangle \leftarrow |000\rangle$) (∼450−550 cm^{-1}) and ($|101\rangle$, $|201\rangle \leftarrow |000\rangle$) (∼700−800 cm^{-1}) bands have been assigned.

6 Conclusion

The electronic structure of ($^1A_1$) NaH_2^+ has been investigated using all-electron, relativistically-corrected CCSD(T). At this level of theory, the D_0 energy for the

[($^1A_1$) $NaH_2^+ \rightarrow$ ($^1S_0$) $Na^+ +$ ($^2A_1$) H_2 ($v = 0$)] dissociation reaction was calculated to be 10.3 kJ mol^{-1}, and as such is in excellent agreement with the experimental value of 10.3 ± 0.8 kJ mol^{-1} [13]. Vibration band origins and vibration-averaged structures for ($^1A_1$) NaH_2^+, ($^1A'$) $NaHD^+$ and ($^1A_1$) NaD_2^+ were calculated using an embedded 118-point CCSD(T) PES in conjunction with variational algorithms. The character of ground and excited state vibrational eigenvectors were assessed using a configuration weight assignment scheme. In the case of ($^1A'$) $NaHD^+$, it was observed that the low-lying vibrational states possessed a relatively delocalised nature. The rovibrational structure of the NaH_2^+ $v_{HH} = 1 \leftarrow v_{HH} = 0$ band was calculated and compared to that of the isovalent species LiH_2^+. The strengths of the Li^+/Na^+-H_2 ($v_{HH} = 0$) and Li^+/Na^+-H_2 ($v_{HH} = 1$) interactions were discussed in the context of the vibrational red shifts of these bands. Vibrational radiative properties, such as vibration transition moments, Einstein A and B coefficients, vibration band strengths and radiative lifetimes were calculated using an embedded 90-point CCSD(T) DMS. All transition moment integrals were calculated using a novel numerical scheme. Spectral transition intensities of all rovibrational states such that $v \leq 10$ and $J \leq 5$ were subsequently calculated for each species. In all cases, the rovibrational wave functions of ($^1A_1$) NaH_2^+, ($^1A'$) $NaHD^+$ and ($^1A_1$) NaD_2^+ were assigned unequivocally using the J, K_a and K_c assignment scheme, in conjunction with normal modes of vibration.

Acknowledgments The authors wish to acknowledge support from the Australian Partnership for Advanced Computing (APAC), the Australian Centre for Advanced Computing and Communications (AC3) and the high-performance computing facility of The University of Newcastle, Australia. A.J.P. wishes to acknowledge support from the Australian postgraduate award scheme.

References

1. Gianturco FA, Giorgi PG, Berriche H, Gadea FX (1996) Astron Astrophys Supp Ser 117:377
2. Sanz C, Bodo E, Gianturco FA (2005) Chem Phys 314:135
3. Page AJ, von Nagy-Felsobuki EI (2008) J Mol Struct (Theochem) 853:53
4. Burrows A, Volobuyev M (2003) Astrophys J 583:985
5. Page AJ, von Nagy-Felsobuki EI (2007) J Phys Chem A 111:4478
6. Kraemer WP, Spirko V (2006) Chem Phys 330:190
7. Emmeluth C, Poad BLJ, Thompson CD, Weddle GH, Bieske EJ (2007) J Chem Phys 126:204309
8. Thompson CD, Emmeluth C, Poad BLJ, Weddle GH, Bieske EJ (2006) J Chem Phys 125:044310
9. Papousek D, Aliev M (1982) Molecular vibration-rotation spectra. Elsevier, Prague
10. Switalski JD, Huang JTJ, Schwartz ME (1974) J Chem Phys 60:2252
11. Falcetta MF, Pazun JL, Dorko MJ, Kitchen D, Siska PE (1993) J Phys Chem 97:1011
12. Curtiss LA, Pople JA (1988) J Phys Chem 92:894
13. Bushnell JE, Kemper PR, Bowers MT (1994) J Phys Chem 98:2044
14. Tamassy-Lentei I, Szaniszlo J (2000) J Mol Struct (Theochem) 501:403
15. Barbatti M, Jalbert G, Nascimento MAC (2001) J Chem Phys 114:2213
16. Vitillo JG, Damin A, Zecchina A, Ricchiardi G (2005) J Chem Phys 122:114311
17. Page AJ, von Nagy-Felsobuki EI (2008) Chem Phys 351:37
18. Page AJ, von Nagy-Felsobuki EI (2007) Mol Phys 105:2527
19. Roos BO, Veryazov V, Widmark P (2004) Theor Chem Acc 111:345
20. Woon DE, Dunning TH (1994) J Chem Phys 100:2975
21. Dunning TH (1989) J Chem Phys 90:1007
22. Douglas M, Kroll NM (1974) Ann Phys (NY) 82:89
23. Hess BA (1986) Phys Rev A 33:3742
24. Wells B, Wilson S (1983) Chem Phys Lett 101:429
25. Werner H-J, Knowles PJ, Lindh R, Manby FR, Schütz M, Celani P, Korona T, Rauhut G, Amos RD, Bernhardsson A, et al (2006) MOLPRO, v. 2006.1, a package of ab initio programs. http://www.molpro.net
26. Carney GD, Langhoff SR, Curtiss LA (1977) J Chem Phys 66:3724
27. Harris DO, Engerholm GG, Gwinn WD (1965) J Chem Phys 43:1515
28. Watson JKG (1968) Mol Phys 15:479
29. Burton PG, von Nagy-Felsobuki E, Doherty G, Hamilton M (1984) Chem Phys 83:83
30. Searles DJ, von Nagy-Felsobuki EI (1988) Am J Phys 56:444
31. Strang G, Fix GJ (1973) An analysis of the finite element method. Prentice-Hall, New-Jersey
32. Searles DJ, von Nagy-Felsobuki EI (1991) J Chem Phys 95:1107
33. Sudarko, Hughes JM, von Nagy-Felsobuki EI (2000) Aust J Phys 53:665
34. Zare RN (1987) Angular momentum. Wiley, New York
35. Dixon DA, Gole JL, Komornicki A (1988) J Phys Chem 92:1378
36. Searles DJ, von Nagy-Felsobuki EI (1991) Phys Rev A 43:3365
37. Searles DJ, von Nagy-Felsobuki EI (1991) In vibrational spectra and structure. Elsevier, New York
38. Searles DJ, von Nagy-Felsobuki EI (1992) Comp Phys Commun 67:527
39. Searles DJ, von Nagy-Felsobuki EI (1991) Ab initio calculations of vibrational band origins. Elsevier, New York
40. Jordan KD, Kinsey JL, Silbey R (1974) J Chem Phys 61:911
41. Jorish VS, Scherbak NB (1979) Chem Phys Lett 67:160
42. Pardo A, Camacho JJ, Poyato JML (1986) Chem Phys Lett 131:490
43. Ogilvie JF (1981) Proc Roy Soc London Ser A A378:387
44. Forsythe GE, Malcolm MA, Moler CB (1977) Computer Methods for Mathematical Computations. Prentice-Hall, New York
45. Gabriel W, Reinsch E-A, Rosmus P, Carter S, Handy NC (1993) J Chem Phys 99:897
46. Fink U, Wiggins T, Rank D (1965) J Mol Spec 18:384
47. Wolniewicz L (1966) J Chem Phys 45:515